ELSEVIER

Catalysis Today 51 (1999) 47–57

CATALYSIS TODAY

Amorphous features of working catalysts

Yuan Kou[a,*], Hong-li Wang[b], Hui Zhang[a], Xi-yao Yang[a]

[a]*College of Chemistry and Molecular Engineering, Peking University, Beijing 100871, China*
[b]*Dalian Institute of Chemical Physics, Chinese Academy of Sciences, Dalian 116023, China*

Abstract

In this paper, we review our recent considerations regarding the structural features of active ensembles and/or sites in supported oxide catalysts. The unusual and sometimes unique catalytic properties of these catalyst systems are believed to be intimately related to the amorphous nature of the catalyst structure. Surface coordination geometry is a good concept or starting point to depict the nature and to correlate the structure of a working catalyst with its catalytic behavior.

Keywords: Supported oxide catalysts; Structure–activity relationships; Amorphous ensemble; Stable interface; Local coordination; Site-symmetry; Descriptive chemistry

1. Introduction

The structure–reactivity relationship of supported catalysts is a topic that has been dealt with in many previous studies, including a considerable number of in situ studies. The rationalization of the electronic and chemisorptive properties of the catalytic sites requires more detailed knowledge of the geometric arrangement of the surfaces than what is generally available. The lack of suitable techniques to observe the surfaces directly, however, usually limits the depth of the desired characterizations. On the other hand, our understanding seems to be hindered by the lack of a fundamental way to depict the features of the catalyst surfaces. Detailed structures of some single-crystal oxide surfaces have been well known for years [1,2], but few of the many oxide catalysts studied are well considered in the surface/interface geometry sense. Descriptive chemistry of supported catalyst ensembles/particles as well as its influence on catalysis is still not clear as of yet.

This paper reviews our present understanding of the surfaces of some working catalysts at the atomic level. Most of the catalysts discussed here have been previously described in proper journals. The focus of the current review is therefore on the connection of the results obtained, rather than the preparations, catalytic activities and characterizations, in attempting to provide more fundamental and practical understanding of the metal oxide surface science for working catalyst design and improvement.

2. General understanding

We have become accustomed to observing the surfaces of working catalysts by the techniques and descriptive chemistry suitable for crystal research only.

*Corresponding author.

0920-5861/99/$ – see front matter
PII: S0920-5861(99)00007-3

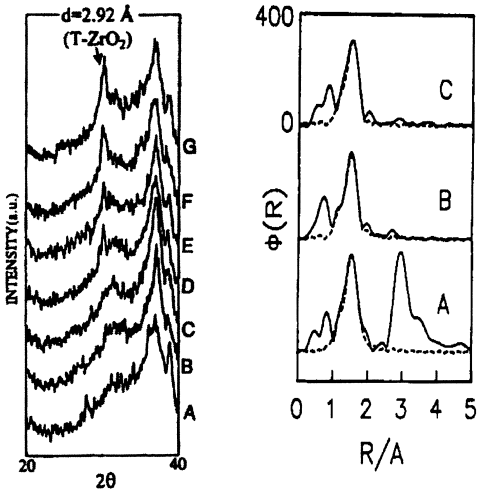

Fig. 1. Left: XRD pattern of (A) γ-Al_2O_3, and (B)–(G) ZrO_2/Al_2O_3 with Zr loading of 3, 5, 7, 15 and 20 wt%. Right: EXAFS-derived Fourier transform for (A) M-ZrO_2, (B) ZrO_2/Al_2O_3 and (C) ZrO_2/Al_2O_3 after use.

Such an approach usually fails to lead to catalyst improvement. Alumina-supported zirconia (ZrO_2/Al_2O_3), an excellent catalyst for the selective synthesis of ethylene from CO and H_2 (CO conversion: 30%, selectivity to ethylene: 70%), is a good example [3]. The stability of this catalyst under reaction conditions, based on a 400 h testing, offers intriguing prospects for commercialization. The XRD pattern generally shows two very strong peaks corresponding to d=0.314 and 0.282 nm for the (1 1 1) face of monoclinic ZrO_2 (M-ZrO_2) and a very strong peak corresponding to d=0.292 nm for the (1 1 1) face of tetragonal ZrO_2 (T-ZrO_2). XRD patterns (left, Fig. 1) of ZrO_2/Al_2O_3 with different Zr loadings clearly show that a peak corresponding to T-ZrO_2 begins to develop when the Zr loading reaches 15 wt% (left, (E)) and is well resolved when the Zr loading is greater than 25 wt% (left, (G)). Quantitative analysis reveals that the ZrO_2/Al_2O_3 with 25 wt% Zr loading yields only 3–5% T-ZrO_2. We therefore tentatively proposed before EXAFS (extended X-ray absorption fine structure) examination that the catalyst with 14% Zr loading was dominated by an amorphous phase consisting of tetragonal-like ZrO_8 units. An improvement to the preparation of the catalyst has since been made. The amorphous feature of the ZrO_2/Al_2O_3 is immediately revealed by the disappearance

Table 1
Zr *K*-edge EXAFS derived structural parameters

Sample	Shell	CN	*R* (nm)	Average *R*	*R*-factor
M-ZrO_2	Zr–O	4.4 (7)	0.2132 (9)		0.14
	Zr–O	2.6 (2)	0.225 (1)	2.18	
ZrO_2/Al_2O_3	Zr–O	4.2 (5)	0.2105 (8)		0.12
	Zr–O	2.7 (5)	0.223 (1)	2.15	
ZrO_2/Al_2O_3	Zr–O	4.2 (7)	0.211 (1)		0.15
After use	Zr–O	2.6 (8)	0.223 (2)	2.16	

of the Zr–Zr coordination shell (the most intense peak in Fig. 1(A)). Zr *K*-edge EXAFS (Fig. 1(B)) shows that only the uniform nearest oxygen shells are observable on the catalyst. Furthermore, to our great surprise, the best fits to the EXAFS of the catalyst (14 wt%) clearly indicate that the coordination of the nearest oxygen neighbors on the ZrO_2/Al_2O_3, either the coordination number (CN) or the Zr–O bond length (R), is completely identical to that of the ZrO_7 units in crystalline M-ZrO_2, as shown in Table 1.

We considered the catalysts as small crystals or crystalline particles for a long time. It is true that some working catalysts are in the crystalline form. One example is a Cu–Zn catalyst [4]. However, even for supported metal catalysts, the surfaces of some metals may at high temperatures be in semifluid states and therefore lacking in definite structure [5]. We therefore suggest that researchers need to carefully check their ''crystalline'' results when they are studying working catalyst.

3. Descriptive surface geometry

The amorphous characteristic of ZrO_2/Al_2O_3, as a general feature of working catalysts, has been mentioned. However, why the surface is dominated by an M-ZrO_2 but not T-ZrO_2 phase still remains unclear. From the point of view of the coordination geometry, both the zirconia are far less similar to the host γ-alumina. Even for an alumina-supported iron oxide system, in which the coordination tendencies of the both oxides are quite similar to each other, it seems clear that the formation of an electrically neutral Fe_2O_3 ensemble on γ-alumina still takes place in a manner very different from the growth of either crystal.

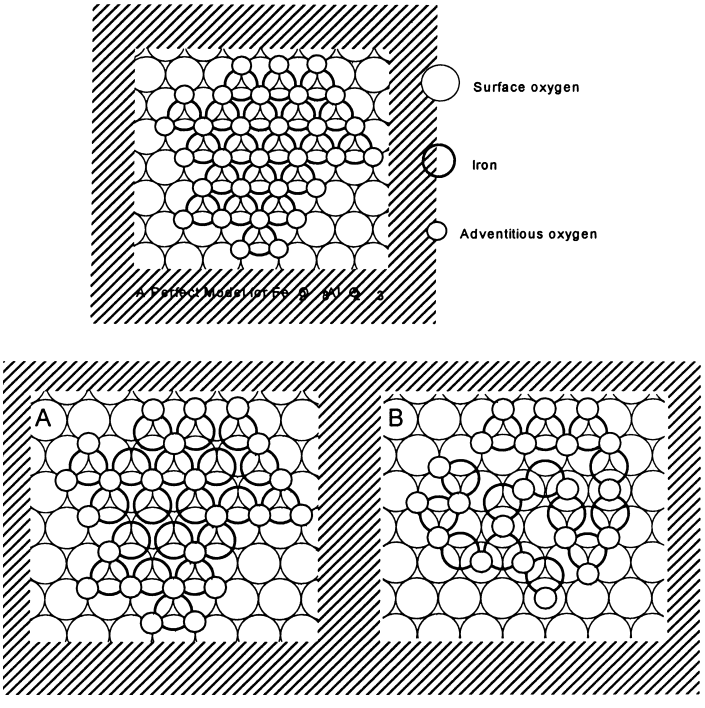

Fig. 2. Perfect Fe_2O_3 monolayer ensemble on the γ-Al_2O_3(1 1 1) face (top) and two derived models for the catalysts: (A) Fe(II)/Al_2O_3 (4.5 wt% Fe); (B) Fe_2O_3/Al_2O_3 (1.5 wt% Fe).

Studies on cluster-derived iron catalyst and an iron oxide catalyst demonstrated that each of the iron cations/atoms tends to appear at a triply bridged, threefold site on oxygen-covered γ-alumina surface [6]. Meanwhile, the iron cation/atom still tends to maintain its six-coordinate, octahedral site-symmetry via sharing of the adsorbed carbon monoxides or the adventitious oxygens with the other iron atoms. The surface carbonyl cluster $Fe_3(\mu_3\text{-CO})CO_6$ [7] or surface oxide ensemble $Fe_{20}O_{30}$ [8] is therefore formed. It is noteworthy that neither the cluster nor the ensemble in that case is absolutely simple duplication of the target pure compound at all. An example of a perfect surface ''molecule'' of Fe_2O_3 is shown in the top of Fig. 2.

It can be seen from the ''molecule'' model that the coordination number of the oxygen is six for each iron site, and that only one type of the nearest iron neighbors appears at 0.295 nm. When oxygen defects are considered, Fig. 2(A) shows that the model changes to an active F–T synthesis catalyst Fe(II)/Al_2O_3 (4.5 wt% Fe) with an apparent formula of $Fe_{20}O_{24}$, a mixture of FeO and Fe_3O_4. When iron defects are taken into account, Fig. 2(B) shows that one more type of adjacent iron neighbors at 0.34 nm is available besides that at 0.295 nm. The model thus changes to a well-defined catalyst Fe_2O_3/Al_2O_3 (1.5 wt% Fe) with an apparent formula of $Fe_{14}O_{21}$ [8].

We need not highlight all the structural details in this review based on the space limitation. We have noticed from the above discussion that the perfect model $Fe_{20}O_{30}$ on alumina, which matches the so-called monolayer structure perfectly, is not obtained from the preparation. The ensembles we obtained are only two samples having defects. Their two-dimensional sizes are less than 2 nm.

4. Percolation theory

It is significant that experimentally obtained coverages of M_2O_3-type transition metal oxides on the surfaces of metal oxides are generally very low, only about 50–70% of the calculated monolayer coverages

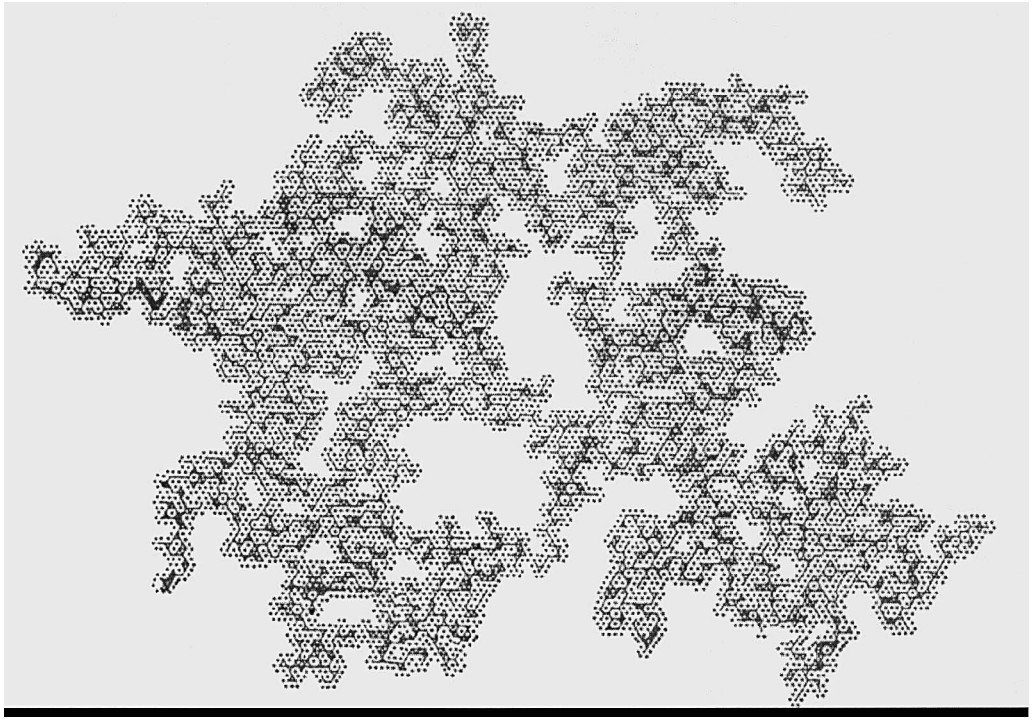

Fig. 3. Percolation theory-derived close-packed model at two-dimensional coverage threshold [11].

[9]. The reason, however, has not been adequately explained by chemists. In fact, the percolation theory formulated by physicists can be extended to account for their dispersion behavior as well [10]. Study on site percolation probability has predicted that a coverage threshold of about 0.5 is certain for a two-dimensional, close-packed system if the interaction between the sites involved in the system is weak. This is due to its amorphous features. A computational result is shown in Fig. 3 [11]. It is likely that the picture is just what we often observed by TEM for the supported catalysts.

It is worth noticing that the amorphous feature of a working catalyst, either partly or entirely, is the characteristic we are interested in for materials that may exhibit unique properties for catalysis. In order to understand the amorphous features of working catalysts, we have suggested that

1. percolation theory be used to depict the amorphous surfaces. In fact, percolation theory has predicted that close-packed sites cannot reach 100% coverage in a two-dimensional arrangement. The estimated coverage, based on a computational model, is only about 50–60%. Interestingly, this result is in full agreement with the knowledge about the dispersion of transition metal oxides on oxide surfaces [9].
2. Surface coordination geometry of a transition metal center (atom or cation) is a good concept or starting point to correlate the structure of a catalyst with its catalytic behavior. Short-range order is the most important factor in determining the properties of a material. The chemical bond in short-range ordered system is in fact no different from that in the lattice.
3. Molecular orbital theory has explained how the site-geometry determines the generation of orbitals and thus finally determines the oxidation states of the elements in a complex. This is also true of supported oxides. For example, the differences in oxidation states between the Fe_2O_3, Fe_3O_4, and FeO formed on a surface can be regarded as a ''size effect'', i.e., it is the average size that may result in

different oxidation states for the ensembles obtained [9].

5. Three examples

How to describe and prepare a properly dispersed amorphous phase is of particular importance for catalysis. In continuing our discussion, we shall show three examples below attempting to make the screening of the catalysts more rational.

5.1. Iron catalysts for the hydrogenation of CO_2 to lower hydrocarbons [12–15]

This work for the first time reveals a geometrically orderly but amorphous Fe^0–Fe^{n+} system for the formation of both a structurally stable interface and a catalytically active surface on a series of TiO_2, ZrO_2/Al_2O_3, ZrO_2, and CeO_2-supported iron catalysts. EXAFS and Mössbauer results for the supports employed and the catalysts obtained are summarized in Tables 2 and 3. Each iron atom/cation on average is coordinated by four nearest oxygen neighbors at 0.203–0.210 nm depending on the specific support employed. Beyond the nearest oxygen, there are a total of 20–28 iron atoms/cations distributed in an orderly fashion in the range of 0.248–0.480 nm. A little deviation from this ordered structure is found for Fe/TiO_2. It is of particular importance, as revealed by this study, that such ordered amorphous ensembles, of which each is 5 nm in size as revealed by TEM (Fig. 4), show very unusual catalytic activity for activating CO_2 (conversion >60%) to produce lower hydrocarbons (selectivity∼60%). Since the Fe–O bond length is found to monotonically change with the substrate metal–oxygen bond, the ferric/ferrous cations most likely appear at the interface connecting both surface zerovalent iron atoms and the support. Percolation theory has been used for the first time to describe the catalyst interface. A model including atomic details has been developed and found to match either the structural parameters or the reaction results very promisingly.

Following the principle established by Figs. 2 and 3, an amorphous ensemble of Fe_2O_3, which is $Fe_{140}O_{210}$ with two-dimensional size of 5 nm, is obtained on an amorphous oxide support, of which the exposed surface is proposed to be close packed, as shown in Fig. 5(A). On iron oxide surfaces, zerovalent iron layers are formed. Each of the first layer iron atoms shown in Fig. 5(B) originally appears at the threefold position on the surface of amorphous Fe_2O_3. However, through the second layer (Fig. 5(C)) to the third layer (Fig. 5(D)), the natural aggregation of the iron atoms commences and finally leads to the formation of the Fe(1 1 0) face. Further layer growth of the iron atoms will take place until the ratio of Fe^0/Fe^{n+} increases to 4:1, as indicated by Mössbauer. Crystalline signal is thus finally observed by XRD and Mössbauer techniques. An irregular arrangement of iron atoms on the top layer is expected.

However, Fig. 5(D) is enough to understand the geometric behavior of this mixed valence ensemble in detail [15].

1. For each iron atom in the first layer, which is closely connected with the Fe_2O_3 monolayer, three cationic sites at about 0.35 nm are observable. It can be seen that the same geometry exists for these cationic sites.
2. Addition of the further layers of the iron atoms other than the first results in the Fe–Fe distances of 0.248 and 0.40 nm, respectively. For example, for

Table 2
Properties of the supports used

Support	BET surface area (m^2/g)	Monolayer Fe loading (wt%)	XRD analysis	EXAFS-derived metal–oxygen bond length
TiO_2	20	2.8	15% rutile, 85% anatase	Ti *K*-edge, Ti–O: 0.197 nm [12]
ZrO_2/Al_2O_3 (Zr 50 wt%)	187	17.7	Amorphous	Zr *K*-edge, Zr–O: 0.215 nm [13]
ZrO_2	27	3.8	Monoclinic	Zr *K*-edge, Zr–O: 0.218 nm [13]
CeO_2	9	1.3	Cerianite	Ce *K*-edge, Ce–O: 0.228 nm[a]

[a] Not simultaneously determined by this work.

Table 3
Best fits to Fe *K*-edge EXAFS and Mössbauer for the catalysts[a]

Catalyst (proper reduction temperature K)	Shell	CN	*R* (nm)	*R*-factor	Mössbauer (% based on area)
Fe/TiO_2 (773)	Fe–O	3.6 (6)	0.203 (2)	0.09	Fe^0, 17.4
	Fe–Fe	1.4 (4)	0.248 (2)		α-Fe, 22.9
	Fe–Fe	5.8 (15)	0.276 (2)		Fe^{2+}, 10.1
	Fe–Fe	2.7 (20)	0.342 (6)		Fe^{2+} in $FeTiO_3$, 49.6
	Fe–Fe	3.7 (23)	0.398 (4)		
	Fe–Fe	5.8 (28)	0.480 (3)		
$Fe/ZrO_2/Al_2O_3$	Fe–O	4.1 (6)	0.204 (2)	0.07	
(723–773)	Fe–Fe	3.8 (6)	0.248 (1)		α-Fe, 46.2
	Fe–Fe	6.7 (9)	0.275 (1)		Fe^{3+}, 11.4
	Fe–Fe	3.4 (18)	0.346 (4)		Fe_3O_4, 42.4
	Fe–Fe	3.0 (15)	0.401 (3)		
	Fe–Fe	8.5 (32)	0.480 (3)		
Fe/ZrO_2 (723)	Fe–O	4.1 (6)	0.207 (2)	0.07	
	Fe–Fe	3.9 (6)	0.248 (1)		α-Fe, 76.2
	Fe–Fe	6.7 (10)	0.277 (1)		Fe^{3+}, 23.8
	Fe–Fe	3.0 (20)	0.355 (5)		
	Fe–Fe	3.6 (16)	0.400 (3)		
	Fe–Fe	9.9 (40)	0.481 (4)		
Fe/CeO_2	Fe–O	3.6 (10)	0.210 (3)	0.07	
(673–723)	Fe–Fe	4.0 (7)	0.248 (1)		α-Fe, 82.5
	Fe–Fe	7.1 (18)	0.273 (2)		Fe^{3+}, 17.5
	Fe–Fe	3.2 (22)	0.352 (8)		
	Fe–Fe	3.7 (26)	0.398 (5)		
	Fe–Fe	5.1 (30)	0.479 (4)		

CN=coordination number; *R*=shell radius; DW=Debye–Waller factor.
[a] α-Fe phase is predominantly observed by XRD patterns.

the iron atoms in the third layer, three Fe^0 neighbors from the first layer of iron atoms at a distance of ca. 0.4 nm begin to be observable. The same result can be obtained when the first layer of iron atoms are considered to be the central atoms while those in the third layer are regarded as neighbors.

3. Without the influence of the Fe_2O_3 interface, the packing of the top several layers may become more regular. Therefore, a very weak crystalline signal for these zerovalent iron atoms is expected.
4. The sandwich-like ensemble (Fig. 5(D)) consisting of about 500 zerovalent iron atoms and about 120 iron cations is about 5 nm in overall size.
5. Although reconstruction of the layers and rearrangement of the iron atoms may occur, the geometry of the Fe–Fe shells at 0.275 and 0.48 nm changes only slightly. The coordination numbers for these two shells are significantly higher than that of the other shells at 0.248 and 0.35–0.40 nm. Interestingly, the exact distances for the shells at 0.34–0.40 nm may change resulting from the reconstruction and the rearrangement. Therefore, relatively larger errors in distance are understandable for the shells at either 0.34 or 0.40 nm. The Fe–Fe distances found in EXAFS appear to be consistent with those expected from an imperfectly stacked small cubic close packing ensemble with an amorphous nature.

Furthermore, this sandwich model is of particular interest in understanding the catalytic behavior of this series of catalysts. It can be found from Fig. 5(D) that surrounding the border of the ensemble, electronic exchange and coordinate unsaturation between Fe^0 and Fe^{n+} are highly feasible. As briefly mentioned above, it is just what we desired for the catalysts

Fig. 4. TEM of $Fe/ZrO_2/Al_2O_3$. The diameter of the three particles is 5 nm.

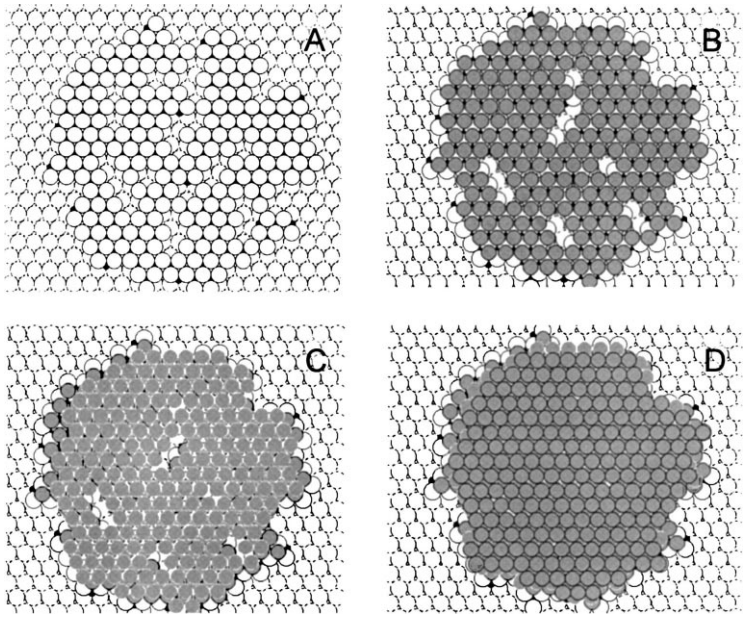

Fig. 5. Geometric models for the formation of (A) amorphous monolayer of Fe_2O_3 (solid circles) amorphous oxide surface (oxygen covered, dashed circles); (B) the first, (C) the second and (D) the third layer of iron atoms.

designed. The catalytic mechanism involved has been found to be closely related to such a structure [15].

5.2. *Silica-supported manganese–tungsten catalyst for the oxidative coupling of methane [16,17]*

The silica-supported manganese–tungsten catalyst, $Mn/Na_2WO_4/SiO_2$ has received increased attention as a catalyst for the oxidative coupling of methane because of its excellent catalytic performance. A C_{2+} selectivity of 65% at 37% methane conversion was reported by Li and co-workers [16]. A C_{2+} selectivity in excess of 80% at a CH_4 conversion of 20% over this catalyst was then repeatedly confirmed by the Lunsford group. Recently, the $Mn/Na_2WO_4/SiO_2$ catalyst has been investigated by using the *L*-edge and the *K*-edge XAFS and XPS [16]. The surface of the fresh catalyst is found to be dominated by oxygen-enriched amorphous phases consisting of discretely distributed tetrahedral WO_4 and octahedral MnO_6 groups. The tungsten in a T_d-center is responsible for the activation of methane while the manganese in an O_h-center is responsible mainly for the transformation and transportation of oxygens. The combination of the two centers can therefore transfer electrons and oxygens simultaneously. It is to be emphasized that the oxygens responsible for the high performance of the $Mn/Na_2WO_4/SiO_2$ in the reaction are not the so-called ''lattice oxygens''. The amorphous structure of the catalyst has effectively converted the lattice oxygens to the active oxygens before the catalysis occurred.

This dual-component catalyst also provides a good example to understand which component must appear at the surface. For the formation of an electronically neutral surface, the WO_4 group does not need to bond with the silica surface very tightly, for example, in a triply bridged mode. In this sense, the study on silica-supported Re_2O_7 is very informative [18]. The reaction of Re_2O_7 with the siloxane bridges leads to the formation of surface perrhenates. For our system, two tungsten ions (W^{6+}) may share one bridging oxygen and each binds to the silica surface via a single oxygen. That is enough to maintain their electroneutrality. Such a group of tungsten species is easily enriches and moves on the surface, and finally will completely disappear from the surface under fluidized bed conditions.

However, when the formation of a neutral surface is considered, the manganese ions have a different story. As indicated by the best fits to the Mn *K*-edge EXAFS, each of the manganese ions on the fresh catalyst is coordinatively saturated by six oxygen neighbors. It means that a single Mn^{3+} cannot exist on the surface unless it is contained in a group of manganese ions or in a system of manganese–tungsten mixture. In both cases, the silica-support must be closely involved since the surface is not enriched in Mn as determined by XPS. For example, when the geometric understanding of $Fe_3(\mu_3\text{-}CO)CO_6$ [7] is applied here, it can be estimated that three Mn^{3+} ions could form a cluster having a formula of either $Mn_3(\mu_2\text{-}O)_3O_3$ or $Mn_3(\mu_3\text{-}O)O_6$. If each of the manganese cations were located in a triply bridged site on surface, it would have a hexa-coordinated, octahedral site-symmetry. Even so, however, they would be stoichiometrically in the form of Mn_3O_6 or Mn_3O_7 with an extremely high electro-negativity (-3 or -5), participation of the sodium cations and/or the formation of $Mn_{20}O_{30}$ ensembles [8] must still be extremely necessary. It is the reason why a significant amount of manganese ions (about 2/5) must be retained in a small crystalline form although their loading (<2 wt%) is not high, and why the surface of the fresh catalyst cannot be enriched in Mn. The other 3/5 manganese ions kept in an amorphous state have to disperse themselves into WO_4 groups and/or the silica substrate by the formation of W–O–Mn bonds or Mn–O–Si bonds.

The amorphous feature of the $Mn/Na_2WO_4/SiO_2$ catalyst has been demonstrated to be responsible for the high performance of the catalyst. Structural studies on crystalline Mn_2O_3 have suggested that the manganese ions tend to maintain a four-coordinated, square planar geometry (D_{4h}) by making two axial oxygen sites empty [19], implying that Mn_2O_3 will be a good oxygen releaser. On the other hand, studies on Na_2WO_4/SiO_2, Na_2WO_4/CeO_2, and $NaMnO_4/SiO_2$ seem to suggest that tetrahedral transition metal sites (T_d) are necessary for the activation of methane. Thus, an active T_d site accompanied with a good oxygen-releaser must be an effective catalytic ensemble for the oxidative coupling of methane. For this study, we have,

$$T_d\text{-}W^{6+} \leftrightarrow D_{4h}\text{-}Mn^{3+} \leftrightarrow O_h\text{-}Mn^{3+}. \quad (1)$$

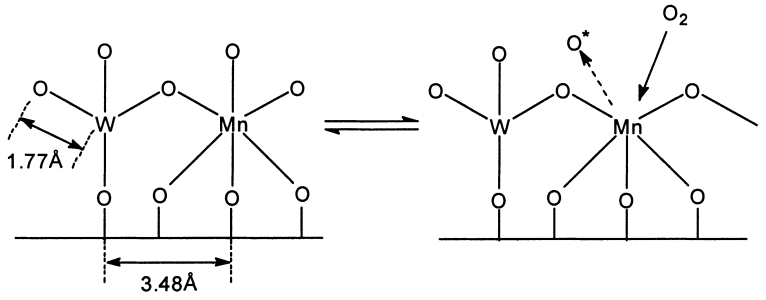

Fig. 6. Two tentative models involving the possible formation of active oxygen species (O^*). Notice: unlike that of WO_4 groups, mononuclear MnO_6 species cannot exist alone on the surface as stated in the discussion. The Mn center shown in the scheme must be stoichiometrically bound into an ensemble of either Mn_2O_3 and/or WO_4–Mn_2O_3–SiO_2 complexes. The situation, however, is not shown for the sake of clarity.

Two tentative structural models involving the possible formation of active oxygen species are considered for the surface ensembles, as shown in Fig. 6.

5.3. *Simultaneous activating of methane and carbon dioxide to give aromatics (SAMCA) [20,21]*

All the oxide-supported iron catalysts showing activity in the hydrogenation of CO_X (X=1, 2) to produce hydrocarbons without exception contain octahedrally coordinate sites [6–8,12–15]. The difference from one to another is only if the sites are coordinatively saturated or not. This indicates that octahedral metallic sites (either iron atoms and/or cations) are generally necessary for the activation of CO_X. It is reasonable to ask the question: if the site-geometry changes from octahedral to tetrahedral, what will happen [17]? We have recently found that tetrahedral catalytic sites on supported oxide catalysts are of particular importance for activating methane [16,20,21]. On the basis of this finding, a series of new catalysts, Fe/SiO_2 and Cr/SiO_2, which consists of two cationic centers with different oxidation states and site-symmetries from each other, has been designed. A novel catalytic route for simultaneous activation of methane and carbon dioxide to give aromatics (SAMCA) has been realized over these catalysts.

In fact, we have been skeptical on the experimental fact for years that by changing the support to amorphous silica, little catalytic activity in the hydrogenation of CO_X is detected for the iron catalyst so obtained. To our surprise, however, the Fe/SiO_2 has been found to be a catalyst for the oxidation of methane, a reverse reaction of CO_X hydrogenation. Further studies confirm that not only Fe/SiO_2 but also Co/SiO_2 and Mn/SiO_2 are active in oxidative coupling of methane but inert in CO_2 hydrogenation to produce hydrocarbons. This unusual finding encourages us to propose that the tetrahedral metallic cations on silica surfaces are most likely responsible for the completely reversed catalytic behavior. In this regard, a series of 3d-metal oxides containing predominantly tetrahedral MO_4 sites (M=Mn, Fe, Co) has been successfully prepared and characterized [17]. Fe K-edge XANES spectra clearly indicate that the final states and the coordination of the iron ions on the Na–Fe/SiO_2 is virtually identical to that observed in iron (Fe^{3+})-containing silica glass in which the site-symmetry of the iron species is predominantly tetrahedral. Very promisingly, in comparison with the precursor Fe/SiO_2 (C_2 yield: 0.7%), reaction studies show that the Na–Fe/SiO_2 (and the Na–Co/SiO_2 and Na–Mn/SiO_2) exhibits a significantly increased OCM activity in terms of either the selectivity or the total yield (2.5%) for C_2 hydrocarbons. This completely reversible behavior may be crudely described by the following reaction:

$$CO_X \underset{\text{Oxidation, } T_d\text{--Fe}}{\overset{\text{Hydrogenation, } O_h\text{--Fe}}{\rightleftharpoons}} CH_4. \quad (2)$$

It offers an intriguing opportunity for simultaneous activation of methane and carbon dioxide by presenting both tetrahedral and octahedral centers on surface, i.e.,

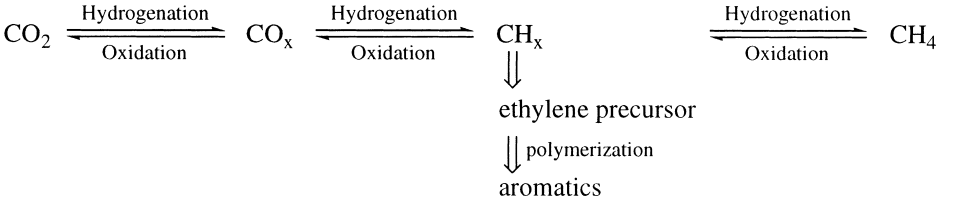

(3)

Table 4
Initial activity of the catalyst in SAMCA

Catalyst	Fe (wt%)	Na (wt%)	BET (m^2/g)	Conversion (%)		Selectivity (%)			Yield (%)[a]
				CH_4	CO_2	C_2	Ar	CO	(C_2+Ar)
Fe/SiO_2	1	0	202.4	3.5	39.0	1.8	3.9	94.2	0.2
$Na–Fe/SiO_2$	1	1	0.8	1.8	12.3	6.1	34.4	59.5	0.7

Reaction conditions: 0.4 MPa, 840°C, CH_4/CO_2=7:5, 20–23 ml/min.
[a] Based on CH_4.

Scheme (3) shows that three processes, hydrogenation of CO_2, oxidative coupling of methane and ethylene polymerization can be perfectly carried out in one step.

Table 4 shows that $Na–Fe/SiO_2$ is considerably more effective in SAMCA than Fe/SiO_2. It is just what we have expected to happen for the reaction of SAMCA. The OCM activity observed over the catalysts and the structural identification of the aromatics obtained from CH_4 and $^{13}CO_2$ suggest that both methane and carbon dioxide are being activated over the adjacent tetrahedral and octahedral sites under the SAMCA conditions. In the meantime, following the same approach, a new catalytic system by presenting both $CrO_4^=$ and Cr_2O_3 on a silica surface has been most recently designed. The selectivities of 4.8% and 48.7% to C_{2^-} and aromatics, respectively, have been achieved over a 7.5 wt% Cr/SiO_2 catalyst at corresponding 3.8% CH_4 and 16.0% CO_2 conversions. To summarize, the importance of the short-range order of the discrete metallic ions dispersed on the supported catalysts is revealed. A new catalytic route, SAMCA, is for the first time realized over the systems designed. An amorphous catalyst structure appears to be necessary for the reaction realized. The findings described here open up a good prospect in gaining insight into the mechanism and the atomic details for catalytic activation of methane and the other small molecules.

6. Conclusion

The working catalyst system consisting of transition metal oxides supported on another oxide often exhibits amorphous features heretofore seldom noticed by the catalyst researchers. This amorphous state arises from the disruption of long-range order because of two-dimensional character and high dispersion of, or presence of defects and vacancies in the catalyst ensembles introduced during the process of preparation. The unusual and sometimes unique catalytic properties of these catalyst systems are believed to be intimately related to the amorphous nature of the catalyst structure, and are worth being vigorously explored. Meanwhile, local coordination environment and oxidation states of the discrete metallic ions on the surface may play a crucial role in catalytic performance. There is a continuing need to develop better model surfaces [22]. Surface coordination geometry is a good concept or starting point to depict the features of the surfaces/interfaces and to correlate the structure of a working catalyst with its catalytic behavior. In this regard, XAFS (including XANES and EXAFS)

appears to be a powerful tool, in combination with others, suitable for the characterization of such working catalyst systems.

Acknowledgements

The authors wish to express their heartfelt thanks to many collaborators at the State Key Laboratory for Oxo Synthesis and Selective Oxidation (Lanzhou) and the State Key Laboratory of Catalysis (Dalian), especially to Associate Profs. Jian-Zhong Niu and Bing Zhang at Lanzhou and Professor Li-Wu Lin at Dalian. We are very grateful to the Photon Factory in Tsukuba, Japan, for use of the BL-7C facilities. We thank Prof. T. Tanaka (Kyoto University) and Prof. M. Nomura (PF) for experimental assistance. We thank Profs. T. Tanaka, S. Yoshida, Y. Iwasawa, S.-K. Shen, and D.W. Goodman for helpful discussion and suggestion. We thank Prof. F.S. Stone for his very critical scientific comments on the original papers prepared for [6–8].

References

[1] V.E. Henrich, Rep. Prog. Phys. 48 (1985) 1481.
[2] V.E. Henrich, P.A. Cox, The Surface Science of Metal Oxides, Cambridge University Press, Cambridge, 1994.
[3] Y. Kou, G.-Q. Su, W.-Z. Zhang, Y.-Q. Yin, J. Catal. 162 (1996) 361.
[4] H.-L. Wang, Y. Kou, Unpublished results.
[5] G.C. Bond, Acc. Chem. Res. 26 (1993) 490.
[6] Y. Kou, H.-L. Wang, M. Te, T. Tanaka, M. Nomura, J. Catal. 141 (1993) 660.
[7] Y. Kou, Z.-H. Suo, H.-L. Wang, J. Catal. 149 (1994) 247.
[8] Y. Kou, H.-L. Wang, J.-Z. Niu, W.-J. Ji, J. Phys. Chem. 100 (1996) 2330.
[9] Y.-C. Xie, Y.-Q. Tang, Adv. Catal. 37 (1990) 1.
[10] R. Zallen, The Physics of Amorphous Solids, Wiley–Interscience, New York, 1983.
[11] P.L. Leath, G.R. Reich, J. Phys. C 11 (1978) 4017.
[12] Y. Kou, Z.-H. Suo, J.-Z. Niu, W.-Z. Zhang, H.-L. Wang, Catal. Lett. 35 (1995) 271.
[13] Y. Kou, Z.-H. Suo, J.-Z. Niu, W.-Z. Zhang, H.-L. Wang, Catal. Lett. 35 (1995) 279.
[14] Z.-H. Suo, Y. Kou, J.-Z. Niu, W.-Z. Zhang, H.-L. Wang, Appl. Catal. 148 (1997) 301.
[15] X. Ren, Ph.D. Thesis, Lanzhou Institute of Chemical Physics, Chinese Academy of Sciences (1997).
[16] Y. Kou, B. Zhang, J.-Z. Niu, S.-B. Li, H.-L. Wang, T. Tanaka, S. Yoshida, J. Catal. 173 (1998) 399.
[17] H. Zhang, J.-Z. Niu, Y. Kou, T. Tanaka, S. Yoshida, J. Solid State Chem. 137 (1998) 325.
[18] S.L. Scott, J.-M. Basset, J. Am. Chem. Soc. 116 (1994) 12069.
[19] C.L. Christ, Descriptive Crystal Chemistry, Wiley, New York 1989.
[20] H. Zhang, Ph.D. Thesis, Lanzhou Institute of Chemical Physics, Chinese Academy of Sciences (1998).
[21] Y. Kou, H.-L. Wang, in Proceedings of the 5th China-Japan Bilateral Symposium on Effective Utilization of Carbon Resources, Plenary-3, Chengdu, China (1997).
[22] M.A. Barteau, Chem. Rev. 96 (1996) 1413.